

## Article

# Marine-Derived Biowaste Conversion into Bioceramic Membrane Materials: Contrasting of Hydroxyapatite Synthesis Methods

Yusuf Wibisono <sup>1,2,\*</sup> , Alien Yala Pratiwi <sup>1</sup>, Christine Ayu Octaviani <sup>1</sup>, Cut Rifda Fadilla <sup>1</sup> , Alfian Noviyanto <sup>3,4,\*</sup>, Epi Taufik <sup>5</sup> , Muhammad K.H. Uddin <sup>6</sup> , Fajri Anugroho <sup>7</sup> and Nurul Taufiqu Rochman <sup>8</sup>

<sup>1</sup> Department of Bioprocess Engineering, Brawijaya University, Jl. Veteran, Malang 65145, Indonesia; alinyalauw@gmail.com (A.Y.P.); christineayuoc@gmail.com (C.A.O.); cutrifda977@gmail.com (C.R.F.)

<sup>2</sup> MILI Institute for Water Research, Kawasan Industri Jababeka, Bekasi 17530, Indonesia

<sup>3</sup> Nano Center Indonesia, Jl. PUSPIPTEK Tangerang Selatan, Banten 15314, Indonesia

<sup>4</sup> Department of Mechanical Engineering, Mercu Buana University, Jl. Meruya Selatan, Kebun Jeruk, Jakarta Barat 11650, Indonesia

<sup>5</sup> Faculty of Animal Science, IPB University, Bogor 16680, Indonesia; epitaufik@apps.ipb.ac.id

<sup>6</sup> Department of Science of Dental Materials, Dr. Ishrat-UI-Ebad Khan Institute of Oral Health Sciences, DOW University of Health Sciences, Karachi 74200, Pakistan; khawaja.hammad@duhs.edu.pk

<sup>7</sup> Department of Environmental Engineering, Brawijaya University, Jl. Veteran, Malang 65145, Indonesia; fajri.anugroho@ub.ac.id

<sup>8</sup> Research Center for Metallurgy and Materials, Indonesian Institute of Sciences, PUSPIPTEK Tangerang Selatan, Banten 15314, Indonesia; nuru006@lipi.go.id

\* Correspondence: Y\_Wibisono@ub.ac.id (Y.W.); a.noviyanto@nano.or.id (A.N.); Tel.: +62-341-571708 (Y.W.)



**Citation:** Wibisono, Y.; Pratiwi, A.Y.; Octaviani, C.A.; Fadilla, C.R.; Noviyanto, A.; Taufik, E.; Uddin, M.K.H.; Anugroho, F.; Rochman, N.T. Marine-Derived Biowaste Conversion into Bioceramic Membrane Materials: Contrasting of Hydroxyapatite Synthesis Methods. *Molecules* **2021**, *26*, 6344. <https://doi.org/10.3390/molecules26216344>

Academic Editor: Teresa Poerio

Received: 13 September 2021

Accepted: 18 October 2021

Published: 20 October 2021

**Publisher's Note:** MDPI stays neutral with regard to jurisdictional claims in published maps and institutional affiliations.



**Copyright:** © 2021 by the authors. Licensee MDPI, Basel, Switzerland. This article is an open access article distributed under the terms and conditions of the Creative Commons Attribution (CC BY) license (<https://creativecommons.org/licenses/by/4.0/>).

**Abstract:** Marine-derived biowaste increment is enormous, yet could be converted into valuable biomaterial, e.g., hydroxyapatite-based bioceramic. Bioceramic material possesses superiority in terms of thermal, chemical, and mechanical properties. Bioceramic material also has a high level of biocompatibility when projected into biological tissues. Tuning the porosity of bioceramic material could also provide benefits for bioseparation application, i.e., ultrafiltration ceramic membrane filtration for food and dairy separation processes. This work presents the investigation of hydroxyapatite conversion from crab-shells marine-based biowaste, by comparing three different methods, i.e., microwave, coprecipitation, and sol-gel. The dried crab-shells were milled and calcinated as calcium precursor, then synthesized into hydroxyapatite with the addition of phosphates precursors via microwave, coprecipitation, or sol-gel. The compound and elemental analysis, degree of crystallinity, and particle shape were compared. The chemical compounds and elements from three different methods were similar, yet the degree of crystallinity was different. Higher Ca/P ratio offer benefit in producing a bioceramic ultrafiltration membrane, due to low sintering temperature. The hydroxyapatite from coprecipitation and sol-gel methods showed a significant degree of crystallinity compared with that of the microwave route. However, due to the presence of Fe and Sr impurities, the secondary phase of  $\text{Ca}_9\text{FeH}(\text{PO}_4)_7$  was found in the sol-gel method. The secondary phase compound has high absorbance capacity, an advantage for bioceramic ultrafiltration membranes. Furthermore, the sol-gel method could produce a snake-like shape, compared to the oval shape of the coprecipitation route, another benefit to fabricate porous bioceramic for a membrane filter.

**Keywords:** bioceramic; ultrafiltration membrane; marine biowaste; hydroxyapatite; microwave; coprecipitation; sol-gel; membrane porosity; sintering

## 1. Introduction

The abundance of marine-derived biowaste or fishery-processing by-products needs to be addressed in search of a sustainable circular economy [1]. From an ecological point of view, the elimination of marine-derived biowaste is in the line with 2030 Sustainable

Development Goals Strategies. This conversion into biomaterials could generate new valuable products, invent new technology and create new business [2–4]. Hydroxyapatite (HAp) is a valuable biomaterial that could be derived from fishery-processing by-products and marine-derived biowaste [5,6].

Hydroxyapatite is a form of calcium phosphate [ $\text{Ca}_{10}(\text{PO}_4)_6(\text{OH})_2$ ] that has been extensively utilized as an implant material and has a composition similar to natural hard tissues such as bone and teeth. It has exceptional biocompatibility, osteoconductivity, and osteoinductivity [7,8]. In addition, many studies have shown that HAp ceramics possess no toxicity and no inflammatory effect [9,10]. Therefore, HAp has been extensively used to replace bone tissues, dental implants, tissue engineering, drug carrier, and biosensor applications [11].

Apart from the renowned utilization of HAp in biomedical application [12], tuning HAp into porous materials could be employed for bioceramic membrane filter for separation of gaseous [13,14], aqueous [15–17], and biological substances [18–20]. When fabricated as bioceramic membrane filters, tailored sintering processes are required to produce specific membrane porosity and tortuosity [21–24]. The high adsorption capacity of HAp can also be embedded in polymeric materials for wide-range separation [25–29]. The incorporation of HAp particles into polymeric mixed matrix ultrafiltration membranes could enhance permeability and rejection of the membranes [30,31]. Based on those promising results, HAp-based ultrafiltration membranes could also be used to enhance selectivity and isolation of specific compounds, for instance, oligosaccharides from milk [32–34]. The application particularly can promote economic benefit in the food industry [35].

HAp can be synthesized in various routes and can be derived from synthetic and natural resources. Synthetic HAp syntheses methods, e.g., precipitation [36], radiofrequency thermal plasma [37], the sol–gel method [38], and hydrothermal methods [39]. However, these methods usually use hazardous chemicals, aging processes, and an imbalanced stoichiometric ratio [40]. Apart from many attempts that have been conducted to use a more environmentally friendly chemical, natural materials have been widely used, e.g., bovine bones [41], fish bones [42], fish scales [43], oyster shells [44], corals [45], eggshells [46], and crab shells [47]. The advantages are twofold—the reduced biowaste and the production of value-added materials.

In this study, we developed HAp from crab shells through microwave, coprecipitation, and sol–gel methods. Producing HAp from crab shells is a low-cost and easy process. Additionally, crab by-products are abundant in Indonesia, since crab is one of Indonesia's main export commodities. About 25–50% of the total crab bioproduct mass is in the form of crab shells [47]. Crab shells contain around 40–70% calcium carbonate, depending on the species [48]. In many studies, calcium carbonate as a calcium source can be processed further to synthesize hydroxyapatite [49–51]. By comparing the results from three different processes—microwave, coprecipitation, and sol–gel methods—this study aimed at investigating the most effective process and economically efficient methods to produce HAp, especially for bioceramic ultrafiltration membranes.

## 2. Results and Discussion

A series of HAp characterization was conducted to examine the results of conversion through microwave, coprecipitation, and sol–gel methods. As described in the Methods Section (Section 3), investigation on the molecular structure, chemical composition, crystallinity, and microstructural morphology were conducted, and the results are presented here.

### 2.1. Molecular Structure

Vibrational spectroscopy, i.e., FTIR is susceptible to detect HAp molecular structure, through vibrational frequencies related to HAp chemical bonds [52]. Figure 1 displays the FTIR of HAp synthesized by microwave (Figure 1a), coprecipitation (Figure 1b), and sol–gel (Figure 1c). From FTIR spectra, hydroxyapatite materials have been successfully produced

by the presence of  $\text{PO}_4^{3-}$  and  $\text{OH}^-$  anions. Phosphate ion absorbance was observed in wave number  $963\text{ cm}^{-1}$  with vibration  $\nu_1$   $\text{PO}_4^{3-}$  ion within wave number  $1059\text{ cm}^{-1}$  and  $1100\text{ cm}^{-1}$  caused by vibration  $\nu_3$   $\text{PO}_4^{3-}$  ion. All samples showed their peak at a wavenumber of  $1459\text{ cm}^{-1}$ , indicating the presence of  $\text{CO}_3^{2-}$  anion. The presence of  $\text{CO}_3^{2-}$  ion was caused by the interaction between the samples and air during synthesis processes. The  $\text{CO}_3^{2-}$  vibration at  $1446\text{ cm}^{-1}$  corresponded with aragonite and calcite. At the temperature of  $1000\text{ }^\circ\text{C}$ , the presence of  $\text{OH}^-$  was higher than that of  $600\text{ }^\circ\text{C}$ , indicating that the  $\beta$ -tcp phase was mainly produced. The higher temperature could decrease the carbonate groups.

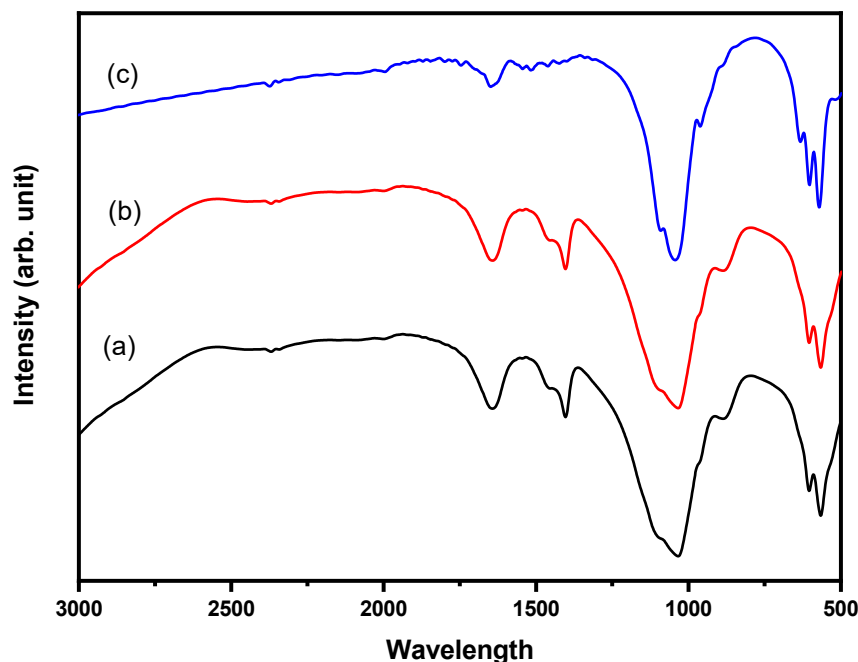


**Figure 1.** FTIR of HAp synthesized by (a) microwave, (b) coprecipitation, and (c) sol-gel.

The FTIR results agreed with the FTIR analysis reported in the literature. Bending vibration of phosphate appeared at  $465$ ,  $559$ , and  $598\text{ cm}^{-1}$ , while the band appeared at  $962$ ,  $1022$ , and  $1088\text{ cm}^{-1}$ , due to stretching vibration [53]. Another report stated that the peaks at  $430$ ,  $524$ ,  $581$ ,  $896$ ,  $994$ ,  $1064$ , and  $1128\text{ cm}^{-1}$ , were attributed to the phosphate ions of HAp [54]. Asymmetric stretching vibration  $\nu_3$  due to the presence of  $\text{PO}_4^{3-}$  ion was strongly observed between  $1000$  and  $1150\text{ cm}^{-1}$ , while asymmetric bending vibration  $\nu_4$  of  $\text{PO}_4^{3-}$  ion was observed between  $560$  and  $610\text{ cm}^{-1}$  [55]. The infrared splitting factor which is calculated by the sum of peak intensities at  $604$  and  $566\text{ cm}^{-1}$  divided by the intensity of the valley between them, can show the degree of crystallinity qualitatively [52]. However, the quantification of crystallinity is better measured by using XRD analysis.

## 2.2. Crystallinity and Chemical Composition

Another important HAp property that was measured is the degree of crystallinity using X-ray diffraction (XRD) measurement. The XRD can determine crystalline structures and quality, crystal size, and lattice defect of the HAp grain [56]. At different treatments, crystal growth of HAp as nanocrystalline materials can be measured by XRD analysis [57]. Figure 2 shows the XRD patterns of HAp synthesized by three different methods, including the synthesized CaO from crab shells (Figure 2). This explains that the reaction of CaO with phosphate-based material to form HAp was successful, showing the formation of HAp phases. Obviously, the final phases depended on the synthesis method, for instance, single-phase HAp, can only be obtained swiftly and evenly by synthesizing using the microwave, as shown in Figure 2b. This result agrees with previous reports in which HAp was successfully synthesized by microwave [58–60]. The typical XRD patterns

are similar to those reports, whereby low crystallinity was observed in XRD patterns. Indeed, the crystallinity of HAp could be enhanced by calcination at high temperatures, i.e., >1000 °C [61]; however, the particle size is more likely to grow during calcination.

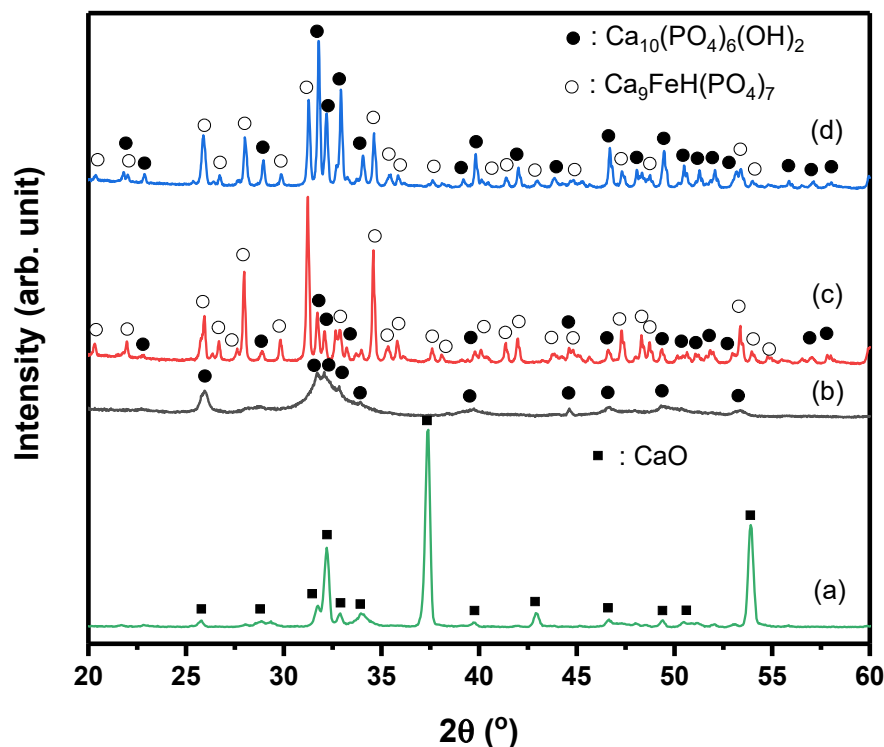


**Figure 2.** XRD patterns of CaO phase (a) and HAp synthesized by (b) microwave, (c) coprecipitation, and (d) sol-gel.

As shown in Figure 2b, the diffractogram peaks were observed at angles  $2\theta$  25.942°, 31.719°, 32.152°, and 32.877°, similar to the standard of JCPDS [62]. However, the crystallinity of microwave HAp was lower, about 25%, compared with the HAp coprecipitation (Figure 2c) and HAp sol-gel (Figure 2d), which were approximately 84% and 92%, respectively.

Nevertheless, the coprecipitation and sol-gel method showed the presence of  $\text{Ca}_9\text{FeH}(\text{PO}_4)_7$  phase, in addition to the HAp phase. Interestingly, the  $\text{Ca}_9\text{FeH}(\text{PO}_4)_7$  phase was dominant in the coprecipitation method, showing the high-intensity peak at 31.2°, even though the calcination temperature was similar to the sol-gel method, i.e., 1000 °C. To verify the presence of Fe impurities, the XRF measurement was conducted.

According to Table 1, the amount of Fe for the three methods was similar, about 1.1 wt.%, while the amount of Ca for microwave, coprecipitation, and sol-gel was 74.35, 78.02, and 79.91 wt.%, respectively. The difference in the Ca content is more likely due to the synthesis method, whereby coprecipitation and sol-gel could maintain the amount higher than 78%. To confirm this result, HAp was synthesized using a microwave at 600 W, and the result showed the amount of Ca and P was 75.94 and 19.6 wt.%, respectively. This indicates that the power of the microwave influences the number of elements. Moreover, the Ca/P ratio of the microwave was the lowest, compared with other methods, i.e., 2.69, as shown in Table 1, while the other method showing the Ca/P ratio > 4. This is the one possible reason that microwave synthesis produces a single-phase HAp. The fabrication of bioceramic ultrafiltration membranes could benefit from the high Ca/P ratio; the details are discussed in Section 2.4 as an outlook.

**Table 1.** Elemental analysis of HAp synthesized by microwave, coprecipitation, and sol–gel.

Methods	Elements (wt.%)									
	Ca	P	Ti	Mn	Fe	Cu	Sr	Zr	Others	Ca/P
Microwave	74.35	21.3	0.074	0.27	1.09	0.066	2.3	0.3	0.250	2.69
Coprecipitation	78.02	17.3	0.063	0.28	1.10	0.068	2.5	0.3	0.369	2.73
Sol–Gel	79.34	16.4	0.068	0.26	1.08	0.065	2.2	0.3	0.287	4.84

However, the microwave method prevented the reaction between Fe and HAp to form  $\text{Ca}_9\text{FeH}(\text{PO}_4)_7$ . It seems the power of microwave used in this study was not enough to induce reaction between Fe and HAp, as characterized by lower crystallinity in Figure 2b compared with Figure 2c,d. As shown in Figure 2b, the main peak of HAp synthesized by microwave was very broad, significantly different from HAp synthesized by coprecipitation (Figure 2c) and sol–gel (Figure 2d). Broadening of the XRD peak indicates that crystallite size decreased. The crystallite size was estimated from peak  $31.719^\circ$  (121). Indeed, the crystallite size of HAp synthesized by microwave was very fine, i.e., 10.3 nm, compared with those coprecipitation and sol–gel, as shown in Table 2.

**Table 2.** Crystallite size, strain, and particle size of HAp synthesized by microwave, coprecipitation, and sol–gel.

Methods	Crystallite Size (nm)	Strain (%)	Particle Size (nm)
Microwave	10.3	0.98	$100 \pm 29$
Coprecipitation	179	0.09	$465 \pm 107$
Sol–Gel	96.7	0.11	$522 \pm 206$

Nevertheless, the broadening of the peak in the XRD of microwave HAp was also influenced by the strain. The crystallite sizes of coprecipitation and sol–gel methods, which were 179 and 96.7 nm, respectively, increased more than nine times, compared with the microwave method.

### 2.3. HAp Microstructure

Figure 3 presents the SEM images of HAp microstructure obtained by three different synthesis methods. Indeed, the HAp synthesized by microwave showed fine microstructure, as shown in Figure 3a and its magnification. The average particle size of microwave HAp was  $100 \pm 29$  nm.

As shown in the magnification of Figure 3a, there are a lot of very fine microstructure microwave HAp which cannot be clearly seen. The planetary or spherical shapes with fewer pores were observed similar to the finding from Lamkhao et al. [63]. It seems that these were HAp particles, and the size was about 10–30 nm, which is almost similar to the crystallite size. This result also confirmed the low crystallinity of microwave HAp, as shown in Figure 2b. However, the microwave HAp synthesis method has several advantages, e.g., rapid heating, less reaction time, and more energy efficiency [64].

In contrast, the microstructure of coprecipitation (Figure 3b) and sol–gel (Figure 3c) experienced grain growth noticeably, compared with microwave HAp. The average particle size of coprecipitation and sol–gel HAp was  $465 \pm 107$  and  $522 \pm 206$  nm, respectively. Although the calcination temperature was similar for the coprecipitation and sol–gel HAp, the size and shape were quite different. Coprecipitation showed an irregular shape, which tended to form an oval shape, as shown in Figure 3b. According to Shojai et al. [65], HAp synthesis using coprecipitation methods could produce several crystalline shapes such as irregular, sphere, rod/needle-like, plate, etc.

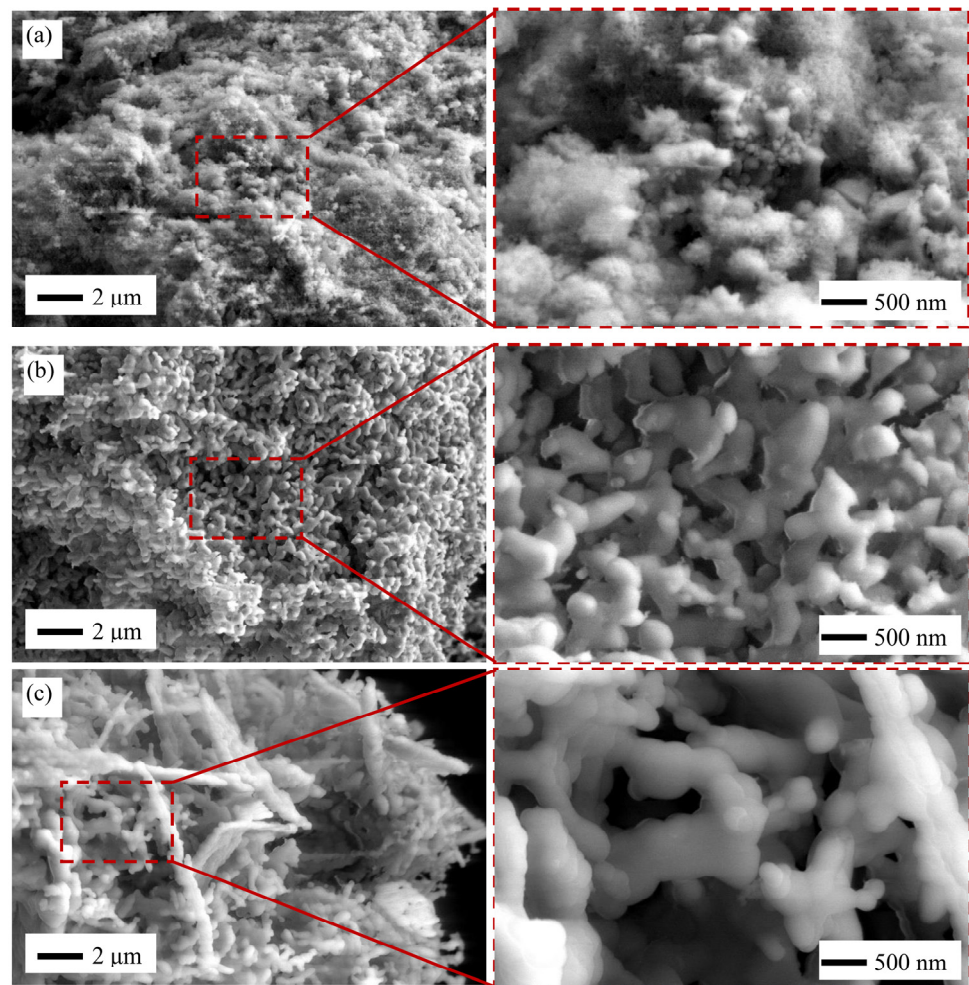


**Figure 3.** SEM images of HAp synthesized by (a) microwave, (b) coprecipitation, and (c) sol-gel with its magnification.

Furthermore, HAp synthesized by the sol-gel method showed a snake-like shape, as shown in Figure 3c. This snake-like shape is reported by Noviyanto et al. [66] while synthesizing nano-sized  $\text{La}_2\text{Ti}_2\text{O}_7$  using chemothermal pulverization. The sol-gel method could produce HAp shapes such as irregular, sphere, and rod/needle tube [65]. Agitation speed, pH, and temperature during HAp synthesis affect the grain size and shape [67].

#### 2.4. An Outlook: Bioceramic Ultrafiltration Membrane Application

When utilized as a biomaterial, HAp must possess a high level of biocompatibility [68], which has a Ca/P ratio is 1.67. However, the purpose of this study was to evaluate the potential use of the HAp as a bioceramic ultrafiltration membrane. The HAp produced by all methods in this study had a higher Ca/P ratio, compared with stoichiometry HAp because it was extracted from natural resources of marine-derived biowaste, i.e., crab shells, resulting in the presence of trace elements responsible for the non-stoichiometric HAp, including the existence of CaO in the HAp produced [69].

As the basic material for bioceramic ultrafiltration membranes, CaO has many advantages. Sintered pure CaO has many micropores, and the pore size could be enhanced by adding some additives [70]. During the sintering process, the dense and crystallized CaO show a low sintering temperature, i.e., below 900 °C, and low dielectric constant, and it has higher flexural strength above 134 MPa [71]. These properties imply that the material is appropriate for bioceramic ultrafiltration membranes. When sintered at a higher temperature such as 1300 °C for 3 h, the pure CaO exhibit the best densification [72]. Tuning

the bioceramic membrane pores by using additives or pore-forming agents could be added in the CaO sintering processes [73–75].

The existence of calcium iron hydrogen phosphate or  $\text{Ca}_9\text{FeH}(\text{PO}_4)_7$  is also another advantage, although its benefit for bioceramic ultrafiltration membranes is still unknown. The compound has a high capability as an absorber from, e.g., in UV light, as cosmeceutical, or used in water or wastewater treatment [76–79].

### 3. Materials and Methods

#### 3.1. Materials

The crab-shell (*Portunus pelagicus*) biowaste as calcium precursor (Figure 4) was obtained from the marine industry in the north coastal line of Pasuruan, East Java, Indonesia. Some chemicals were used in this research, e.g., diammonium phosphate  $(\text{NH}_4)_2\text{HPO}_4$ , hydrochloric acid HCl 37%, phosphoric acid  $\text{H}_3\text{PO}_4$  85%, ammonia  $\text{NH}_3$  25%, and ethanol 96% are purchased from Merck KGaA (Darmstadt, Germany).



**Figure 4.** The dried crab-shell as calcium precursor.

#### 3.2. Preparation of Calcium Oxide

The crab shells were washed to remove remained crab meat and other impurities. The crab shells then dried under open sun drying for 12 h, followed by 4 h of drying in the electric oven until reaching  $9.5 \pm 0.12\%$  wet basis moisture content. The dried crab shells were milled into a fine powder using a pilot-size tubular ball mill (rotation speed 84.6 rpm, 1:10 crab shells, and stainless-steel balls ratio) for 4 h [80]. The produced powder was then sieved using woven wire 325 mesh sieve and produced crab-shell powder with 44  $\mu\text{m}$  in sizes. The sieved powder was further milled with a custom-made Planetary Ball Mill (double 500 mL stainless steel vials, rotation speed 450 rpm) and produced powder with 4.6  $\mu\text{m}$  particle sizes. The obtained powder sample was dissolved in Tween-80 polysorbate surfactant solution and characterized using a particle size analyzer (Malvern Nano-ZS, UK). The powder was then calcinated at a temperature of 1000 °C for 5 h and produced calcium oxide (CaO) powder. The CaO powders were then synthesized into Hap materials by using three different methods, i.e., microwave, coprecipitation, and sol-gel methods, adapted and modified from [65].

#### 3.3. Synthesis of Hydroxyapatite: Microwave

A total of 6.25 g CaO was dissolved in 100 mL HCl 37% 1:3 in beaker glass; then, 262.5 mL of  $(\text{NH}_4)_2\text{HPO}_4$  0.25 M was added to the mixture. The mixture was stirred vigorously for 30 min using a magnetic stirrer (Thermo scientific Cimarec+, Waltham, MA, USA). The pH of the mixture was adjusted to 10–11 by adding 1:1 25% liquor  $\text{NH}_4\text{OH}$  and demineralized water. The mixture was then immediately heated using the microwave at the power of 600 Watt and 800 Watt for 15 min. The precipitate formed was filtered using filter paper with a pore size of approximately 8–11  $\mu\text{m}$  and washed with demineralized water to eliminate the remaining ammonia. It was then dried using an oven (Binder RedLine, Tuttlingen, Germany) at 100 °C for 24 h. Dried HAp precipitate was ground to produce fine powder using mortar and pestle. The step was repeated several times by varying the particle sizes and microwave power [81]. The synthesis condition is summarized in Table 3.

**Table 3.** Hydroxyapatite conversion by microwave, coprecipitation, and sol–gel methods.

Methods	Thermal-Induced Reaction	Time (min)
Microwave	600 W; 800 W	15
Coprecipitation	1000 °C	360
Sol–Gel	1000 °C	360

### 3.4. Synthesis of Hydroxyapatite: Coprecipitation

The coprecipitation method was based on the previous procedure with slight modification [24]. The amount of 22 g of CaO powder was dissolved in demineralized water and mixed with diluted H<sub>3</sub>PO<sub>4</sub> 85% (60 °C, agitation speed 700 rpm). The H<sub>3</sub>PO<sub>4</sub> was added by titration process with a drop rate of 3 mL/minute. NH<sub>3</sub> was then added to the suspension until it reached pH 10. Subsequently, the suspension was then sonicated with an ultrasonic bath (Branson 3510, Brookfield, CT, USA) for 1 h at 42 kHz. The suspension was placed at room temperature for 24 h. The obtained sediment was washed with demineralized water and filtered using filter paper with a pore size of approximately 8–11 µm. The sediment was dried in an oven (Binder RedLine, Tuttlingen, Germany) for 15 h at 90 °C and calcinated at 1000 °C for 6 h. The synthesis condition is summarized in Table 3.

### 3.5. Synthesis of Hydroxyapatite: Sol-Gel

The amount of 7.4 g of CaO powder was dissolved in 100 mL of ethanol 96% and mixed with 100 mL of H<sub>3</sub>PO<sub>4</sub> that has been diluted in demineralized water (temperature of 37 °C, agitation speed of 300 rpm). The H<sub>3</sub>PO<sub>4</sub> was added by titration process with a drop rate of 1 mL/minute. The NH<sub>3</sub> was added to the suspension until it has reached a pH of 10. The suspension was placed at room temperature for 24 h. The obtained gelatin was washed with demineralized water 3 times and then filtered using filter paper with a pore size of approximately 8–11 µm. The sediment was then dried in an oven (Binder RedLine, Tuttlingen, Germany) for 18 h at 105 °C and subsequently calcinated at 1000 °C for 6 h [82]. The synthesis condition is summarized in Table 3.

### 3.6. Characterization of Hydroxyapatite

The HAp powder was then characterized using a Fourier transform-infrared (Shimadzu 8400S, Kyoto, Japan), X-ray diffraction (PANalytical X'Pert3 Powder, Malvern, UK), X-ray fluorescence (PANalytical Minipal 4, Malvern, UK), and scanning electron microscope (FEI Quanta FEG 650, Hillsboro, OR, USA).

## 4. Conclusions

Hydroxyapatite-based bioceramic particles derived from crab shells biowaste were successfully synthesized by using three different methods—microwave, coprecipitation, and sol–gel. Analysis of chemical compounds by FTIR showed that the functional groups from HAp produced from three different routes were similar. Based on the XRD results, the degree of crystallinity of HAp synthesized by using the microwave method was much lower than the other two methods. Elemental analysis using XRF showed that Fe and Sr elements existed and acted as impurities, which lead to the formation of Ca<sub>9</sub>FeH(PO<sub>4</sub>)<sub>7</sub> that was observed in the sol–gel method. CaO as the main constituent offers the best properties as raw material for bioceramic ultrafiltration membranes.

**Author Contributions:** Conceptualization, Y.W., A.N. and E.T.; methodology, Y.W.; formal analysis, Y.W. and A.N.; investigation, C.A.O., A.Y.P. and C.R.F.; data curation, A.N.; writing—original draft preparation, Y.W., A.N., C.A.O., A.Y.P. and C.R.F.; writing—review and editing, Y.W., A.N., E.T., M.K.H.U., F.A. and N.T.R.; supervision, Y.W., A.N. and F.A.; project administration and management, Y.W.; funding acquisition, Y.W., A.N. and E.T. All authors have read and agreed to the published version of the manuscript.

**Funding:** This research was funded by the Ministry of Research and Technology of the Republic of Indonesia/National Research and Innovation Agency, under National Competitive Basic Research

Grant (Penelitian Dasar) scheme No. 197/E4.1/Ak.04.PT/2021 at Universitas Brawijaya, grant number 1270.39/UN10.C10/TU/2021.

**Acknowledgments:** The authors would like to acknowledge Dikianur Alvianto in the project administration.

**Conflicts of Interest:** The authors declare no conflict of interest.

## References

1. Caruso, G.; Floris, R.; Serangeli, C.; Di Paola, L. Fishery Wastes as a Yet Undiscovered Treasure from the Sea: Biomolecules Sources, Extraction Methods and Valorization. *Mar. Drugs* **2020**, *18*, 622. [CrossRef]
2. Maschmeyer, T.; Luque, R.; Selva, M. Upgrading of marine (fish and crustaceans) biowaste for high added-value molecules and bio(nano)-materials. *Chem. Soc. Rev.* **2020**, *49*, 4527–4563. [CrossRef]
3. Rubini, D.; Farisa Banu, S.; Veda Hari, B.N.; Ramya Devi, D.; Gowrishankar, S.; Karutha Pandian, S.; Nithyanand, P. Chitosan extracted from marine biowaste mitigates staphyloxanthin production and biofilms of Methicillin-resistant *Staphylococcus aureus*. *Food Chem. Toxicol.* **2018**, *118*, 733–744. [CrossRef]
4. Uranga, J.; Etxabide, A.; Cabezudo, S.; de la Caba, K.; Guerrero, P. Valorization of marine-derived biowaste to develop chitin/fish gelatin products as bioactive carriers and moisture scavengers. *Sci. Total Environ.* **2020**, *706*, 135747. [CrossRef]
5. Pon-On, W.; Suntornsaratoon, P.; Charoenphandhu, N.; Thongbunchoo, J.; Krishnamra, N.; Tang, I.M. Hydroxyapatite from fish scale for potential use as bone scaffold or regenerative material. *Mater. Sci. Eng. C* **2016**, *62*, 183–189. [CrossRef]
6. Dabiri, S.M.H.; Rezaie, A.A.; Moghimi, M.; Rezaie, H. Extraction of Hydroxyapatite from Fish Bones and Its Application in Nickel Adsorption. *BioNanoScience* **2018**, *8*, 823–834. [CrossRef]
7. Wibisono, Y.; Yuliani, R.; Kamilia, N.; Ardian, D.; Lastriyanto, A.; Rafianto, V.; Diniardi, E.; Sandra. Hybridization of nitrogen compounds and hydroxyapatite: A slowly released fertiliser for water sustainability. *IOP Conf. Ser. Earth Environ. Sci.* **2020**, *475*, 012005. [CrossRef]
8. Sassoni, E. Hydroxyapatite and Other Calcium Phosphates for the Conservation of Cultural Heritage: A Review. *Materials* **2018**, *11*, 557. [CrossRef] [PubMed]
9. Balázsi, C.; Weber, F.; Kövér, Z.; Horváth, E.; Németh, C. Preparation of calcium–phosphate bioceramics from natural resources. *J. Eur. Ceram. Soc.* **2007**, *27*, 1601–1606. [CrossRef]
10. Zakharov, N.A.; Polunina, I.A.; Polunin, K.E.; Rakitina, N.M.; Kochetkova, E.I.; Sokolova, N.P.; Kalinnikov, V.T. Calcium Hydroxyapatite for Medical Applications. *Inorg. Mater.* **2004**, *40*, 641–648. [CrossRef]
11. Kumta, P.N.; Sfeir, C.; Lee, D.-H.; Olton, D.; Choi, D. Nanostructured calcium phosphates for biomedical applications: Novel synthesis and characterization. *Acta Biomater.* **2005**, *1*, 65–83. [CrossRef]
12. Bee, S.-L.; Hamid, Z.A.A. Hydroxyapatite derived from food industry bio-wastes: Syntheses, properties and its potential multifunctional applications. *Ceram. Int.* **2020**, *46*, 17149–17175. [CrossRef]
13. Xiong, Z.-C.; Yang, R.-L.; Zhu, Y.-J.; Chen, F.-F.; Dong, L.-Y. Flexible hydroxyapatite ultralong nanowire-based paper for highly efficient and multifunctional air filtration. *J. Mater. Chem. A* **2017**, *5*, 17482–17491. [CrossRef]
14. Ibrahim, M.; Labaki, M.; Giraudon, J.-M.; Lamonier, J.-F. Hydroxyapatite, a multifunctional material for air, water and soil pollution control: A review. *J. Hazard. Mater.* **2020**, *383*, 121139. [CrossRef] [PubMed]
15. Chang, H.; Park, N.; Jang, Y.; Lim, H.; Kim, W. Application of the hydroxyapatite crystallization-filtration process to recover phosphorus from wastewater effluents. *Water Sci. Technol.* **2020**, *81*, 2300–2310. [CrossRef] [PubMed]
16. Reichert, J.; Binner, J.G.P. An evaluation of hydroxyapatite-based filters for removal of heavy metal ions from aqueous solutions. *J. Mater. Sci.* **1996**, *31*, 1231–1241. [CrossRef]
17. Abo-Almaged, H.H.; Gaber, A.A. Synthesis and characterization of nano-hydroxyapatite membranes for water desalination. *Mater. Today Commun.* **2017**, *13*, 186–191. [CrossRef]
18. Kuiper, M.; Sanches, R.M.; Walford, J.A.; Slater, N.K.H. Purification of a functional gene therapy vector derived from Moloney murine leukaemia virus using membrane filtration and ceramic hydroxyapatite chromatography. *Biotechnol. Bioeng.* **2002**, *80*, 445–453. [CrossRef]
19. Yang, L.; Ning, X.; Chen, K.; Zhou, H. Preparation and properties of hydroxyapatite filters for microbial filtration. *Ceram. Int.* **2007**, *33*, 483–489. [CrossRef]
20. Zhang, C.; Uchikoshi, T.; Liu, L.; Kikuchi, M.; Ichinose, I. Effect of Surface Modification with TiO<sub>2</sub> Coating on Improving Filtration Efficiency of Whisker-Hydroxyapatite (HAp) Membrane. *Coatings* **2020**, *10*, 670. [CrossRef]
21. Lee, Y.; Lee, J.H.; Shin, D.-G.; Noviyanto, A.; Lee, H.-M.; Nishimura, T.; Jang, B.-K.; Kwon, W.-T.; Kim, Y.; Kim, S.; et al. Phase transformation on spark plasma sintered dense polycarbosilane-derived SiC without additive. *Scr. Mater.* **2018**, *143*, 188–190. [CrossRef]
22. Noviyanto, A.; Yoon, D.-H. Metal oxide additives for the sintering of silicon carbide: Reactivity and densification. *Curr. Appl. Phys.* **2013**, *13*, 287–292. [CrossRef]
23. Qureshi, H.F.; Nijmeijer, A.; Winnubst, L. Influence of sol–gel process parameters on the micro-structure and performance of hybrid silica membranes. *J. Membr. Sci.* **2013**, *446*, 19–25. [CrossRef]
24. Wibisono, Y.; Dwijaksara, N.L.B.; Widayatno, W.B.; Wismogroho, A.S.; Amal, M.I.; Rochman, N.T.; Nishimura, T.; Noviyanto, A. Synthesis and Sinterability of Hydroxyapatite from Fishery by-products. *J. Korean Ceram. Soc.* **2018**, *55*, 570–575. [CrossRef]

25. Oprea, M.; Voicu, S.I. Recent Advances in Applications of Cellulose Derivatives-Based Composite Membranes with Hydroxyapatite. *Materials* **2020**, *13*, 2481. [[CrossRef](#)]
26. Pandele, A.M.; Comanici, F.E.; Carp, C.A.; Miculescu, F.; Voicu, S.I.; Thakur, V.K.; Serban, B.C. Synthesis and characterization of cellulose acetate-hydroxyapatite micro and nano composites membranes for water purification and biomedical applications. *Vacuum* **2017**, *146*, 599–605. [[CrossRef](#)]
27. Sivasankari, S.; Kalaivizhi, R.; Gowriboy, N.; Ganesh, M.R.; Shazia Anjum, M. Hydroxyapatite integrated with cellulose acetate/polyetherimide composite membrane for biomedical applications. *Polym. Compos.* **2021**, *42*, 5512–5526. [[CrossRef](#)]
28. Alrafai, H.A.; Ali Al-Ahmed, Z.; Ahmed, M.K.; Afifi, M.; Shoueir, K.R.; Abu-Rayyan, A. The degradation of methylene blue dye using copper-doped hydroxyapatite encapsulated into polycaprolactone nanofibrous membranes. *New J. Chem.* **2021**, *45*, 16143–16154. [[CrossRef](#)]
29. Zhang, Q.-Q.; Zhu, Y.-J.; Wu, J.; Dong, L.-Y. Nanofiltration Filter Paper Based on Ultralong Hydroxyapatite Nanowires and Cellulose Fibers/Nanofibers. *ACS Sustain. Chem. Eng.* **2019**, *7*, 17198–17209. [[CrossRef](#)]
30. Kallem, P.; Bharath, G.; Rambabu, K.; Srinivasakannan, C.; Banat, F. Improved permeability and antifouling performance of polyethersulfone ultrafiltration membranes tailored by hydroxyapatite/boron nitride nanocomposites. *Chemosphere* **2021**, *268*, 129306. [[CrossRef](#)]
31. Nor Suhaida Rasman, S.; Riduan Jamalludin, M.; Najieha Kamarudin, S.; Khadijah Hubadillah, S.; Arif Budiman Pauzan, M.; Hafiz Dzarfan Othman, M. Fabrication and characterization of hydroxyapatite based cow bone polysulfone mixed matrix membrane. *IOP Conf. Ser. Mater. Sci. Eng.* **2021**, *1142*, 012010. [[CrossRef](#)]
32. Luo, J.; Nordvang, R.T.; Morthensen, S.T.; Zeuner, B.; Meyer, A.S.; Mikkelsen, J.D.; Pinelo, M. An integrated membrane system for the biocatalytic production of 3'-sialyllactose from dairy by-products. *Bioresour. Technol.* **2014**, *166*, 9–16. [[CrossRef](#)]
33. Martinez-Ferez, A.; Rudloff, S.; Guadix, A.; Henkel, C.A.; Pohlentz, G.; Boza, J.J.; Guadix, E.M.; Kunz, C. Goats' milk as a natural source of lactose-derived oligosaccharides: Isolation by membrane technology. *Int. Dairy J.* **2006**, *16*, 173–181. [[CrossRef](#)]
34. Martinez-Ferez, A.; Guadix, A.; Guadix, E.M. Recovery of caprine milk oligosaccharides with ceramic membranes. *J. Membr. Sci.* **2006**, *276*, 23–30. [[CrossRef](#)]
35. Urashima, T.; Taufik, E.; Fukuda, K.; Asakuma, S. Recent Advances in Studies on Milk Oligosaccharides of Cows and Other Domestic Farm Animals. *Biosci. Biotechnol. Biochem.* **2013**, *77*, 455–466. [[CrossRef](#)] [[PubMed](#)]
36. Cao, L.-Y.; Zhang, C.-B.; Huang, J.-F. Synthesis of hydroxyapatite nanoparticles in ultrasonic precipitation. *Ceram. Int.* **2005**, *31*, 1041–1044. [[CrossRef](#)]
37. Xu, J.; Khor, K.; Dong, Z.; Gu, Y.W.; Kumar, R.R.; Cheang, P. Preparation and characterization of nano-sized hydroxyapatite powders produced in a radio frequency (rf) thermal plasma. *Mater. Sci. Eng. A-Struct. Mater. Prop. Microstruct. Process.* **2004**, *374*, 101–108. [[CrossRef](#)]
38. Masuda, Y.; Matubara, K.; Sakka, S. Synthesis of Hydroxyapatite from Metal Alkoxides through Sol-Gel Technique. *J. Ceram. Soc. Jpn.* **1990**, *98*, 1255–1266. [[CrossRef](#)]
39. Nathanael, A.J.; Han, S.S.; Oh, T.H. Polymer-Assisted Hydrothermal Synthesis of Hierarchically Arranged Hydroxyapatite Nanoceramic. *J. Nanomater.* **2013**, *2013*, 962026. [[CrossRef](#)]
40. Venkatesan, J.; Lowe, B.; Manivasagan, P.; Kang, K.-H.; Chalisserry, E.P.; Anil, S.; Kim, D.G.; Kim, S.-K. Isolation and Characterization of Nano-Hydroxyapatite from Salmon Fish Bone. *Materials* **2015**, *8*, 5426–5439. [[CrossRef](#)]
41. Haas, R.; Donath, K.; Födinger, M.; Watzek, G. Bovine hydroxyapatite for maxillary sinus grafting: Comparative histomorphometric findings in sheep. *Clin. Oral Implant. Res.* **1998**, *9*, 107–116. [[CrossRef](#)]
42. Ozawa, M.; Suzuki, S. Microstructural Development of Natural Hydroxyapatite Originated from Fish-Bone Waste through Heat Treatment. *J. Am. Ceram. Soc.* **2002**, *85*, 1315–1317. [[CrossRef](#)]
43. Ulfyana, D.; Anugroho, F.; Sumarlan, S.H.; Wibisono, Y. Bioceramics synthesis of hydroxyapatite from red snapper fish scales biowaste using wet chemical precipitation route. *IOP Conf. Ser. Earth Environ. Sci.* **2018**, *131*, 012038. [[CrossRef](#)]
44. Wu, S.-C.; Hsu, H.-C.; Wu, Y.-N.; Ho, W.-F. Hydroxyapatite synthesized from oyster shell powders by ball milling and heat treatment. *Mater. Charact.* **2011**, *62*, 1180–1187. [[CrossRef](#)]
45. Hu, J.; Russell, J.J.; Ben-Nissan, B.; Vago, R. Production and analysis of hydroxyapatite from Australian corals via hydrothermal process. *J. Mater. Sci. Lett.* **2001**, *20*, 85–87. [[CrossRef](#)]
46. Ho, W.-F.; Hsu, H.-C.; Hsu, S.-K.; Hung, C.-W.; Wu, S.-C. Calcium phosphate bioceramics synthesized from eggshell powders through a solid state reaction. *Ceram. Int.* **2013**, *39*, 6467–6473. [[CrossRef](#)]
47. Raya, I.; Mayasari, E.; Yahya, A.; Syahrul, M.; Latunra, A.I. Synthesis and Characterizations of Calcium Hydroxyapatite Derived from Crabs Shells (*Portunus pelagicus*) and Its Potency in Safeguard against to Dental Demineralizations. *Int. J. Biomater.* **2015**, *2015*, 469176. [[CrossRef](#)] [[PubMed](#)]
48. Jun, J.-Y.; Jung, M.-J.; Jeong, I.-H.; Kim, G.-W.; Sim, J.-M.; Nam, S.-Y.; Kim, B.-M. Effects of crab shell extract as a coagulant on the textural and sensorial properties of tofu (soybean curd). *Food Sci. Nutr.* **2019**, *7*, 547–553. [[CrossRef](#)]
49. Rusu, V.M.; Ng, C.-H.; Wilke, M.; Tiersch, B.; Fratzl, P.; Peter, M.G. Size-controlled hydroxyapatite nanoparticles as self-organized organic-inorganic composite materials. *Biomaterials* **2005**, *26*, 5414–5426. [[CrossRef](#)] [[PubMed](#)]
50. Yamaguchi, I.; Itoh, S.; Suzuki, M.; Osaka, A.; Tanaka, J. The chitosan prepared from crab tendons: II. The chitosan/apatite composites and their application to nerve regeneration. *Biomaterials* **2003**, *24*, 3285–3292. [[CrossRef](#)]

51. Yamaguchi, I.; Itoh, S.; Suzuki, M.; Sakane, M.; Osaka, A.; Tanaka, J. The chitosan prepared from crab tendon I: The characterization and the mechanical properties. *Biomaterials* **2003**, *24*, 2031–2036. [[CrossRef](#)]
52. Dal Sasso, G.; Asscher, Y.; Angelini, I.; Nodari, L.; Artioli, G. A universal curve of apatite crystallinity for the assessment of bone integrity and preservation. *Sci. Rep.* **2018**, *8*, 12025. [[CrossRef](#)]
53. Ebrahimi, S.; Stephen Sipaut@ Mohd Nasri, C.; Bin Arshad, S.E. Hydrothermal synthesis of hydroxyapatite powders using Response Surface Methodology (RSM). *PLoS ONE* **2021**, *16*, e0251009. [[CrossRef](#)]
54. Zou, Z.; Liu, X.; Chen, L.; Lin, K.; Chang, J. Dental enamel-like hydroxyapatite transformed directly from monetite. *J. Mater. Chem.* **2012**, *22*, 22637–22641. [[CrossRef](#)]
55. Dhanaraj, K.; Suresh, G. Conversion of waste sea shell (*Anadara granosa*) into valuable nanohydroxyapatite (nHAp) for biomedical applications. *Vacuum* **2018**, *152*, 222–230. [[CrossRef](#)]
56. Londoño-Restrepo, S.M.; Jeronimo-Cruz, R.; Millán-Malo, B.M.; Rivera-Muñoz, E.M.; Rodríguez-García, M.E. Effect of the Nano Crystal Size on the X-ray Diffraction Patterns of Biogenic Hydroxyapatite from Human, Bovine, and Porcine Bones. *Sci. Rep.* **2019**, *9*, 5915. [[CrossRef](#)] [[PubMed](#)]
57. Kostov-Kytin, V.V.; Dyulgerova, E.; Ilieva, R.; Petkova, V. Powder X-ray diffraction studies of hydroxyapatite and  $\beta$ -TCP mixtures processed by high energy dry milling. *Ceram. Int.* **2018**, *44*, 8664–8671. [[CrossRef](#)]
58. Han, J.-K.; Song, H.-Y.; Saito, F.; Lee, B.-T. Synthesis of high purity nano-sized hydroxyapatite powder by microwave-hydrothermal method. *Mater. Chem. Phys.* **2006**, *99*, 235–239. [[CrossRef](#)]
59. Silva, C.C.; Graça, M.P.F.; Valente, M.A.; Goes, J.C.; Sombra, A.S.B. Microwave preparation, structure and electrical properties of calcium–sodium–phosphate biosystem. *J. Non-Cryst. Solids* **2006**, *352*, 3512–3517. [[CrossRef](#)]
60. Siddharthan, A.; Seshadri, S.K.; Kumar, T.S.S. Influence of microwave power on nanosized hydroxyapatite particles. *Scr. Mater.* **2006**, *55*, 175–178. [[CrossRef](#)]
61. Yang, Z.; Jiang, Y.; Wang, Y.; Ma, L.; Li, F. Preparation and thermal stability analysis of hydroxyapatite derived from the precipitation process and microwave irradiation method. *Mater. Lett.* **2004**, *58*, 3586–3590. [[CrossRef](#)]
62. Jenkins, R.; Fawcett, T.G.; Smith, D.K.; Visser, J.W.; Morris, M.C.; Frevel, L.K. JCPDS—International Centre for Diffraction Data Sample Preparation Methods in X-Ray Powder Diffraction. *Powder Diffr.* **1986**, *1*, 51–63. [[CrossRef](#)]
63. Lamkhao, S.; Phaya, M.; Jansakun, C.; Chandet, N.; Thongkorn, K.; Rujijanagul, G.; Bangrak, P.; Randorn, C. Synthesis of Hydroxyapatite with Antibacterial Properties Using a Microwave-Assisted Combustion Method. *Sci. Rep.* **2019**, *9*, 4015. [[CrossRef](#)]
64. Hassan, M.N.; Mahmoud, M.M.; El-Fattah, A.A.; Kandil, S. Microwave-assisted preparation of Nano-hydroxyapatite for bone substitutes. *Ceram. Int.* **2016**, *42*, 3725–3744. [[CrossRef](#)]
65. Sadat-Shojai, M.; Khorasani, M.-T.; Dinpanah-Khoshdargi, E.; Jamshidi, A. Synthesis methods for nanosized hydroxyapatite with diverse structures. *Acta Biomater.* **2013**, *9*, 7591–7621. [[CrossRef](#)] [[PubMed](#)]
66. Noviyanto, A.; Nishimura, T.; Kitano, M.; Ohashi, N. Pulverization of oxide powders utilizing thermal treatment in ammonia-based atmosphere. *J. Eur. Ceram. Soc.* **2016**, *36*, 4083–4088. [[CrossRef](#)]
67. Al-Qasas, N.S.; Rohani, S. Synthesis of Pure Hydroxyapatite and the Effect of Synthesis Conditions on its Yield, Crystallinity, Morphology and Mean Particle Size. *Sep. Sci. Technol.* **2005**, *40*, 3187–3224. [[CrossRef](#)]
68. Büyüksağış, A.; Çiftçi, N. HAP Coatings for Biomedical Applications: Biocompatibility and Surface Protection against Corrosion of Ti, Ti6Al4V and AISI 316L SS. *Prot. Met. Phys. Chem. Surf.* **2020**, *56*, 834–843. [[CrossRef](#)]
69. Mohd Pu'ad, N.A.S.; Koshy, P.; Abdullah, H.Z.; Idris, M.I.; Lee, T.C. Syntheses of hydroxyapatite from natural sources. *Heliyon* **2019**, *5*, e01588. [[CrossRef](#)]
70. Miskufova, A.; Havlik, T.; Bitschnau, B.; Kielski, A.; Pomadowski, H. Properties of CaO Sintered with Addition of Active Alumina. *Ceramics-Silikáty* **2015**, *59*, 115–124.
71. Chen, G.-H. Effect of replacement of MgO by CaO on sintering, crystallization and properties of MgO–Al<sub>2</sub>O<sub>3</sub>–SiO<sub>2</sub> system glass-ceramics. *J. Mater. Sci.* **2007**, *42*, 7239–7244. [[CrossRef](#)]
72. Kalita, S.J.; Bose, S.; Hosick, H.L.; Bandyopadhyay, A. CaO–P<sub>2</sub>O<sub>5</sub>–Na<sub>2</sub>O-based sintering additives for hydroxyapatite (HAp) ceramics. *Biomaterials* **2004**, *25*, 2331–2339. [[CrossRef](#)] [[PubMed](#)]
73. Yin, X.; Guan, K.; Gao, P.; Peng, C.; Wu, J. A preparation method for the highly permeable ceramic microfiltration membrane—Precursor film firing method. *RSC Adv.* **2018**, *8*, 2906–2914. [[CrossRef](#)]
74. Hu, Z.; Yang, Y.; Chang, Q.; Liu, F.; Wang, Y.; Rao, J. Preparation of a High-Performance Porous Ceramic Membrane by a Two-Step Coating Method and One-Step Sintering. *Appl. Sci.* **2019**, *9*, 52. [[CrossRef](#)]
75. Azaman, F.; Muhamad Nor, M.A.A.; Wan Abdullah, W.R.; Razali, M.H.; Che Zulkifli, R.; Ahmad Zaini, M.A.; Ali, A. Review on natural clay ceramic membrane: Fabrication and application in water and wastewater treatment. *Malays. J. Fundam. Appl. Sci.* **2021**, *17*, 62–78. [[CrossRef](#)]
76. Onoda, H.; Sasaki, K. Iron, Copper, and Nickel Removal with Calcium Hydrogen Phosphate and Calcium Pyrophosphates in Solution. *Univers. J. Mater. Sci.* **2017**, *5*, 59–63. [[CrossRef](#)]
77. Runge, K.; Blumberga, A.; Blumberga, D. Bioeconomy Growth in Latvia. System-dynamics Model for High-value Added Products in Fisheries. *Energy Procedia* **2017**, *113*, 339–345. [[CrossRef](#)]

78. Piccirillo, C.; Rocha, C.; Tobaldi, D.M.; Pullar, R.C.; Labrincha, J.A.; Ferreira, M.O.; Castro, P.M.L.; Pintado, M.M.E. A hydroxyapatite-Fe<sub>2</sub>O<sub>3</sub> based material of natural origin as an active sunscreen filter. *J. Mater. Chem. B* **2014**, *2*, 5999–6009. [[CrossRef](#)]
79. Rozaini, M.Z.H.; Wai, H.H.C.P.; Razali, M.H.; Osman, U.M.; Anuar, S.T.; Soh, S.K.C.; Ghazali, S.R.B.; Ibrahim, N.H.; Fei, L.C.; Rahmah, S. Calcium Hydroxyapatite-Based Marine Origin: Novel Sunscreen Materials for Cosmeceutical Treatments. *Orient. J. Chem.* **2018**, *34*, 2770–2776. [[CrossRef](#)]
80. Wibisono, Y.; Rafianto, V.; Alvianto, D.; Bagus Hermanto, M. Prediction of size reduction by batch ball milling process for crab shell powder prior hydroxyapatite conversion. *IOP Conf. Ser. Earth Environ. Sci.* **2020**, *542*, 012011. [[CrossRef](#)]
81. Sajahan, N.A.; Wan Ibrahim, W.M.A. Microwave Irradiation of Nanohydroxyapatite from Chicken Eggshells and Duck Eggshells. *Sci. World J.* **2014**, *2014*, 275984. [[CrossRef](#)] [[PubMed](#)]
82. Hidayat, T. *Synthesis and Characterization of Hydroxyapatite Derived from Asian Green Mussel Shell by Sol-Gel Method (in Bahasa Indonesia)*; IPB University: Bogor, Indonesia, 2013.